

Tomographic Volumetric Additive Manufacturing of Silicon Oxycarbide Ceramics

Max Kollep, Georgia Konstantinou, Jorge Madrid-Wolff, Antoine Boniface, Lorenz Hagelüken, Pradeep Vallachira Warriam Sasikumar, Gurdial Blugan, Paul Delrot, Damien Loterie, Juergen Brugger, and Christophe Moser*

Ceramics are highly chemically, thermally, and mechanically resistant. These remarkable properties make them useful across multiple industries; but also, difficult to mold into complex shapes. A possibility to make convoluted ceramic parts is to use preceramic polymers (PCPs) in liquid form. The PCP resin is first solidified in a desired geometry and then transformed into ceramic compounds through a pyrolysis step that preserves the shape. Light-based additive manufacturing (AM) is a promising route to achieve solidification of the PCP resin. Different approaches, such as stereolithography, have already been proposed but they all rely on a layer-by-layer printing process which limits printing speed and object geometry. Herein, the fabrication of complex 3D centimeter-scale ceramic parts by using tomographic volumetric printing is presented, which is fast and offers a high-resolution and geometrical design freedom. First, a photosensitive polysiloxane preceramic resin that is solidified by projecting light patterns from multiple angles is formulated. Then, the obtained 3D printed parts are converted into ceramics by pyrolysis. The strength of this approach is demonstrated through the fabrication of smooth, dense microcomponents exhibiting overhangs and hollow geometries without the need of supporting structures. Their resistance to thermal stress and harsh chemical treatments is characterized.

(e.g., ceramic thermal barrier coatings, filters, lightweight space mirrors, hip or knee implants).^[1–6]

However, the fabrication of complex ceramic parts remains very challenging. Mainly because of their hardness and brittleness, conventional manufacturing processes, such as machining or molding, are limited to simple object geometries as well as being costly and time-consuming. Additive manufacturing (AM) represents an attractive alternative. Not only does it offer more flexibility in terms of architecture and significantly reduce material waste but also it leads to cost-effective production in a shorter time. In the liquid-based AM technologies being used for the fabrication of ceramics, the process starts with a liquid preceramic polymer (PCP) that is first solidified into a 3D object: the so-called green body. The latter is then transformed into a ceramic material, generally denoted as polymer-derived ceramic (PDC), through a pyrolysis step.^[7] Initially, PCP resins were processed or shaped using conventional

polymer-forming techniques such as injection molding or extrusion. Later, it was demonstrated that by adding a photoinitiator to the liquid precursor, the solid green body can be formed by exposure to UV radiation.^[8] Through photopolymerization, laser-based stereolithography (SLA) has enabled the fabrication of PCP components with high resolution and a good surface quality.^[9] It consists of scanning a laser beam on the photosensitive PCP resin and selectively hardening the material, building the 3D green body

1. Introduction


Over the past decades, ceramics have attracted much interest for their superior properties, including hardness, durability, and stability in extreme environments. They meet fabrication needs in various fields ranging from transportation industry (e.g., diesel engines) to the energy sector (e.g., nuclear) but also environment, defense, aerospace, and in the medical sector

M. Kollep, G. Konstantinou, J. Madrid-Wolff, A. Boniface, C. Moser
Laboratory of Applied Photonics Devices
École Polytechnique Fédérale de Lausanne (EPFL)
CH-1015 Lausanne, Switzerland
E-mail: christophe.moser@epfl.ch

L. Hagelüken, J. Brugger
Microsystems Laboratory
École Polytechnique Fédérale de Lausanne (EPFL)
CH-1015 Lausanne, Switzerland

P. V. W. Sasikumar, G. Blugan
Laboratory for High Performance Ceramics
Swiss Federal Laboratories for Material Science and Technology (Empa)
CH-8600 Duebendorf, Switzerland

P. Delrot, D. Loterie
Readily3D SA
EPFL Innovation Park Bâtiment A, CH-1015 Lausanne, Switzerland

 The ORCID identification number(s) for the author(s) of this article can be found under <https://doi.org/10.1002/adem.202101345>.

© 2022 The Authors. Advanced Engineering Materials published by Wiley-VCH GmbH. This is an open access article under the terms of the Creative Commons Attribution-NonCommercial License, which permits use, distribution and reproduction in any medium, provided the original work is properly cited and is not used for commercial purposes.

DOI: 10.1002/adem.202101345

voxel by voxel. A faster variant of SLA is digital light processing (DLP) in which a projector is used to selectively expose and cross-link an entire layer of UV-curable preceramic monomers at once.^[10–12] Using this DLP approach it is possible to print in a few tens of minutes complex scaffold structures like Kelvin cell structures of typical size $5 \times 5 \times 5 \text{ mm}^3$ with a resolution of 50–100 μm that maintain their initial shape during pyrolysis at temperatures of 1000 °C, or large geometries at high print speed using high-area rapid printing.^[9] Two-photon photopolymerization (2PP) is yet another lithography-based AM process characterized by its very high resolution and accuracy, making it ideal for the manufacture of microscopic structures. Pham et al. reported the fabrication of complex SiCN ceramic microstructures with a submicron resolution via nanostereolithography of a PCP.^[13] The process is based on the two-photon absorbed cross-linking of the photosensitive PCP. Later, more complex structures were also reported using the commercial 2PP system by Nanoscribe with higher pyrolysis temperatures.^[14,15] Recently, AM of ceramic components has been demonstrated by gel-casting and filling with ceramic precursors.^[16]

Volumetric 3D printing is a class of emerging light-based technology that eliminates the need for support struts by printing the whole object at once within a resin's container (see illustration in Figure 1a). Volumetric 3D printed objects are self-supported within the build volume and are built in a few tens of seconds as opposed to the tens of minutes required by layer-by-layer systems. The reason for this decreased building time is that the resin does not have to flow to fill in the surface of the build plate when a new layer is cured as done in SLA or DLP. The essence of volumetric 3D printing departs from this layer-by-layer scheme by producing a 3D dose of light within the whole volume of resin using tomographic back projections^[17–19] or orthogonal dual-wavelength photopolymerization.^[20] Tomographic volumetric additive manufacturing is not only faster but also forms isotropic homogeneous polymerized bodies because the whole object is polymerized at once.^[18] Furthermore, this printing approach allows the fabrication of convoluted hollow structures and geometries with large overhangs which are unprintable with other conventional AM techniques. Recent progress in volumetric additive manufacturing now allows printing different materials including acrylic,^[19] thiol-ene photore-sins,^[21] or even scattering resins,^[22] but to our knowledge the 3D printing of ceramics with a tomographic approach has not been reported yet.

2. Results

2.1. Tomographic Printing of Preceramic Resins

Here, we report on the volumetric additive manufacturing of silicon oxycarbide (SiOC) ceramic centimeter-scale components using a polysiloxane ceramic precursor with a cross-linker. Photopolymerization was induced by tomographic back projection. The resin used in the printer is composed of a polysiloxane (SPR 684) with 1,4-butanediol-diacylate (BDDA) as cross-linker. The photoinitiator diphenyl-(2,4,6-trimethylbenzoyl)-phosphin-oxide (TPO) is added as the light sensitive component to trigger the polymerization. The radical polymerization mechanism illustrated in Figure 1b begins with single-photon absorption by the

photoinitiator (TPO). This generates the primary radicals (C-centered acyl and P-centered phosphinoyl radicals) after the α -cleavage of the C–P bond.^[23,24] The efficiency of the cross-linking at the propagation step is enhanced thanks to BDDA. In fact, the primary radicals of the initiation step (TPO) activate the radical polymerization of the BDDA by cleaving the methylene bond. The high reactivity of BDDA correspondingly assists the chain growth of the PCP by a similar mechanism of methylene cleavage. In this way, the cross-linking propagates to a direction perpendicular to the chain of the PCP and should terminate after irradiation stops.

In the volumetric printer, parts are printed within rotating glass vials filled with the photocurable resin as a set of light patterns are exposed onto it (Figure 1a). To ensure high printing fidelity with the target object, it is crucial that the projected light patterns propagate through the resin without being distorted nor attenuated. Regarding this point, the resin is highly transparent and presents only little absorbance coming from TPO, as shown in Figure S1a–c, Supporting Information. Although relatively low, this attenuation can hinder the printability of centimeter-scale shapes (Figure S1d, Supporting Information); thus, we correct for it following the method described in the study by Madrid-Wolff et al.^[22] Also, the resin we use has a viscosity of 873 mPa s, as shown in Figure S2a–b, Supporting Information, which is high enough to prevent sinking of the polymerized part within the printing times of 30–60 s (see Figure S2c–e, Supporting Information). The acrylate-mediated photopolymerization exhibits a thresholded response to light dose^[25] (Figure S1b, Supporting Information). This is the result of two effects: the gelation threshold of the resin^[26] and the presence of an inhibitor in the resin. The inhibitor, here oxygen naturally dissolved from the atmosphere in the resin, reacts with the excited photoinitiator, preventing the initiation of the polymerization process. This nonlinear response of the resin to light is fundamental in tomographic volumetric additive manufacturing; it ensures the projection of several light patterns over a few (at least one) vial's rotation before the solidification of the resin occurs.

2.2. Ceramization of the Polysiloxane Substituted Precursor

The green body is converted to the PDC through the pyrolytic transformation. The SPR-684 is a commercially available polysiloxane which converts to ceramic for pyrolysis temperatures tested already in the range of 1000–2000 °C.^[15,27–31]

Pyrolysis leads to the decomposition of some organic units with an escape of volatile gases. Polymer-to-ceramic conversion usually occurs within a temperature window of 400–800 °C. Ceramic conversion is almost complete above 600 °C and later there will be rearrangement of bonds to form Si–C-rich and Si–O-rich regimes. In our case, pyrolysis plays a key role in the stability of the final structure as both the siloxane and acrylate units have different pyrolysis profile. The acrylate starts to decompose around 375 °C and care must be given at this temperature to avoid formation of bubbles and cracking of structures. Heating should be as slow as possible to allow a smooth escape of volatile units resulting from the decomposition of acrylate units. The pyrolysis profile is designed accordingly (see Supporting Information). The preceramic green bodies

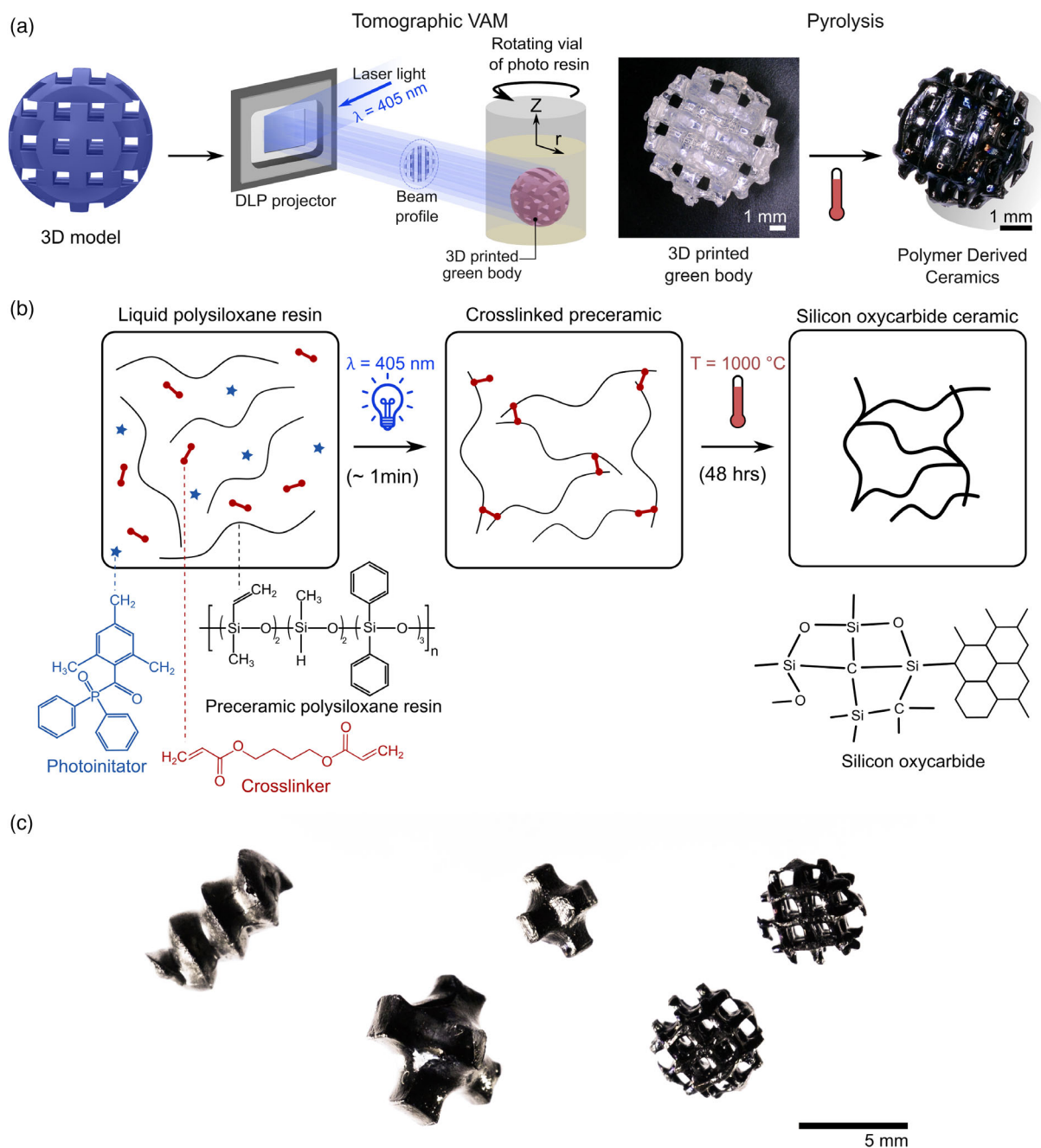


Figure 1. a) In tomographic volumetric additive manufacturing of silicon oxycarbide ceramics, the 3D model of the desired part is used to calculate a set of light patterns which are projected onto a rotating vial filled with a photocurable preceramic resin. The resulting solid green body is retrieved from the liquid resin, and pyrolyzed at $T = 1000^\circ\text{C}$. b) Schematic representation at the molecular level. A polysiloxane preceramic resin is mixed with a cross-linker and a photoinitiator. After excitation with blue light, a stiff network of polymerized and cross-linked polysiloxane chains forms the green body. During a 48 h pyrolysis process, different organic compounds volatilize while the part transforms the part into a silicon oxycarbide ceramic amorphous network.^[10] c) Exemplary 3D printed PDCs. From left to right, a screw with a central hollow channel, two 3D crosses of different sizes, and two spherical woodpiles. Scale bar: 5 mm.

are slowly heated to the specified temperature and a holding step of 1 h is applied at 375°C . This is followed by a heating ramp to 1000°C and kept at the peak temperature for 1 h to complete the ceramic formation. This causes a large mass loss and leads to shrinkage between the green body and the PDC. More details are provided in Figure S3, Supporting Information.

2.3. Geometrical Characterization of 3D Printed Ceramic Parts

Tomographic additive manufacturing is a very flexible technique in terms of object's geometry as it offers the possibility of fabricating microcomponents with unique shapes that may potentially be very challenging to obtain with other AM

technologies. As depicted in Figure 1c, examples of three different shapes with different sizes were successfully printed (from left to right: a screw with three full revolutions and with a channel going down its center, 3D crosses, and a ten-level spherical woodpile structure). We noticed that all these structures were successfully pyrolyzed without major bubble formation, deformation, or cracks. This shows that relatively large objects can be produced especially if their geometries present sufficient escape routes to facilitate degassing, like inner channels.

Hereafter, we characterize the geometry of a PDC woodpile of size $5 \times 5 \times 5 \text{ mm}^3$ with five layers of rods of square cross section measuring $1 \times 1 \text{ mm}$ and spaced out by voids of the same dimensions, as shown in Figure 2a,b. Micro-CT scans show that the parts retained the design voids inside, even after pyrolysis. A ceramic part was cut and the internal side was imaged by a scanning electron microscope (SEM) with 5 nm resolution. In Figure 2b, the SEM image of this part shows that the prints have no signs of porosity through the bulk of the PDC. Small residues can be observed on the same image because of the cutting process.

Figure 2c shows a series of SEM images of the woodpile structure, highlighting the surface quality of the prints. It is visible that the vertical walls of the PDC exhibit some striations when compared to the horizontal ones. These striations are typical of volumetric additive manufacturing and might come from self-writing waveguide effects.^[32,33] Additionally, volumetric additive manufacturing simplifies postprocessing of the green bodies due to the absence of a build plate or support structures. This imaging indicates that the resulting PDC are dense and have smooth surfaces.

Shrinkage poses a difficulty to fabricate functional pieces from PCPs.^[34] Recent works measured the resulting shrinkage after pyrolysis and applied corrections to the 3D model to obtain accurate parts.^[35] Such corrections are more straightforward if the shrinkage is isotropic. Previous works on volumetric additive manufacturing have shown that tomographic back projection results in isotropic, smooth polymerization, contrary to extrusion-based printing and DLP.^[18] As the green bodies are formed volumetrically, without a preferential direction, it is expected that the shrinkage is isotropic. Indeed, the pyrolyzed parts

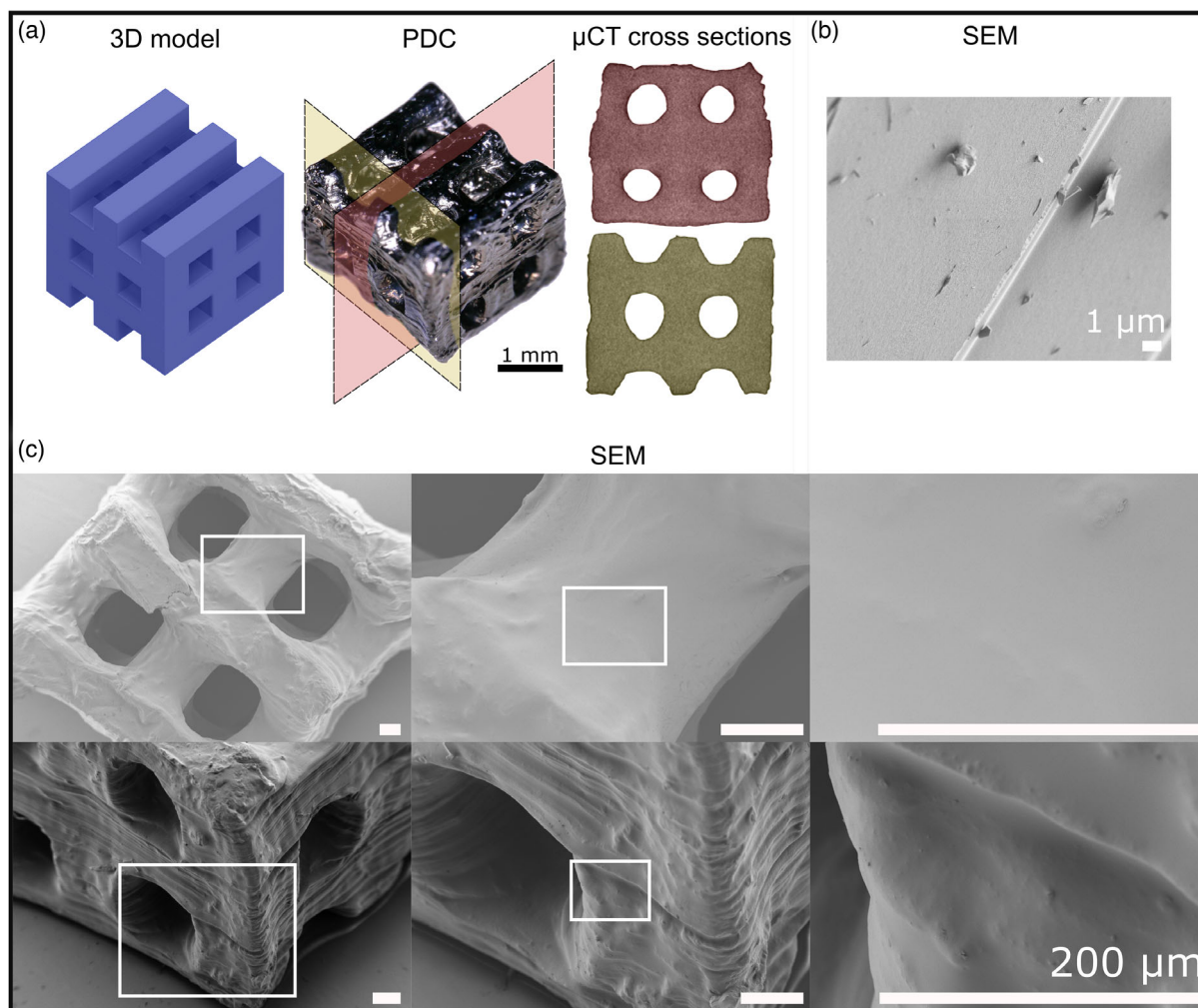


Figure 2. Density and smoothness. a) 3D model, microscope image, and cross sections from micro-CT images of a five-level woodpile. Scale bar: 1 mm. b) SEM image of the internal side of a cleaved ceramic part. c) SEM images of the printed parts and their surfaces. Scale bar: 200 μm.

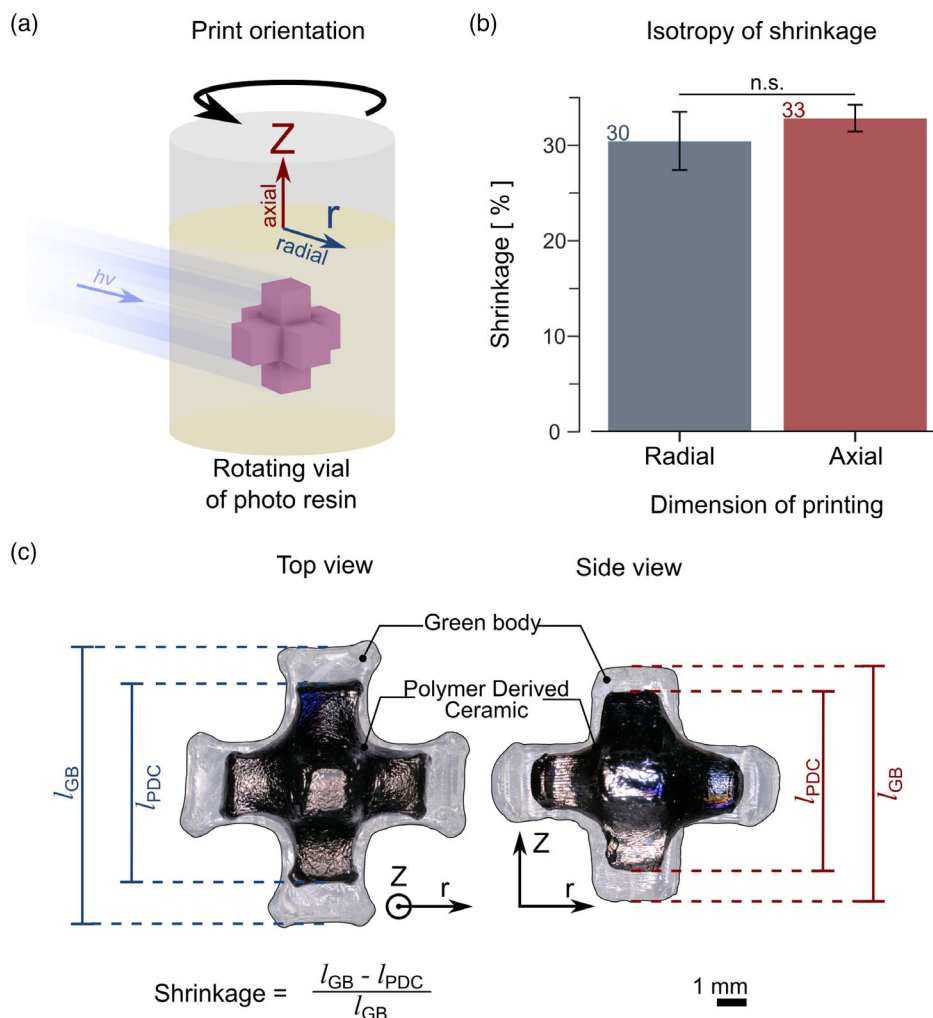


Figure 3. Isotropy of shrinkage. a) In tomographic volumetric additive manufacturing, the object is printed upon the simultaneous polymerization of the resin in the rotating vial. Unlike SLA or DLP, the part exhibits isotropic polymerization along cylindrical coordinates. b) Shrinkage along the axial and radial dimensions of prints. An unpaired *t*-test shows that there is no significant difference between the shrinkage along the radial and axial dimensions. Error bars indicate a standard deviation. c) Overlay of the green body and PDC of a 3D cross.

did not show significant differences in shrinkage along any direction ($p = 6.3 \times 10^{-6}$). This allows the PDCs to keep their shape along the axial and radial dimensions of printing, as shown in **Figure 3**. Additionally, we report a shrinkage of $31.0 \pm 1.7\%$ and a mass loss of $54.0 \pm 0.2\%$ from printing to pyrolysis. These results are in line with those of previous works.^[6,34]

2.4. Materials Characterization

In order to have a detailed and in-depth understanding of the ceramization, we performed a set of different measurements on both green and ceramic parts, namely, Fourier-transform infrared spectroscopy (FTIR), Raman spectroscopy, and X-ray photoelectron spectroscopy (XPS).

In **Figure 4a**, the FTIR spectra of the green and pyrolyzed state are presented. In the spectrum of the green body, several bands are observed which are mostly referred to the organic siloxane

backbone and its functional groups. In the pyrolyzed state, the bands appear as a smoother curve presenting mainly Si—O- and Si—C-type bonds after ceramization. Both spectra are in good agreement with prior work of the exact same PCP in the green state, including the added cross-linker and photoinitiator,^[27,30,36–42] and in the pyrolyzed state.^[27,31,36] As shown in **Figure 4b**, Raman spectroscopy of green bodies and pyrolyzed parts suggests a conversion from an organic to an inorganic material after pyrolysis. The spectrum of the green body shows numerous narrow bands, characteristic of the organic siloxane backbone and cross-linker. Most notably, peaks at 618, 998, 1188, and 1592 cm^{-1} are likely those of the phenyl group in the backbone.^[33,43] The Raman spectrum of the pyrolyzed parts mainly exhibits two broad bands at 1380 and 1600 cm^{-1} , namely, the D and G bands of free carbon.^[44,45] So-called free carbon intrusions have been previously documented in pyrolyzed PDCs.^[46–48] The organization of this free carbon phase segregated within the microstructure and the gradual degradation of the amorphous

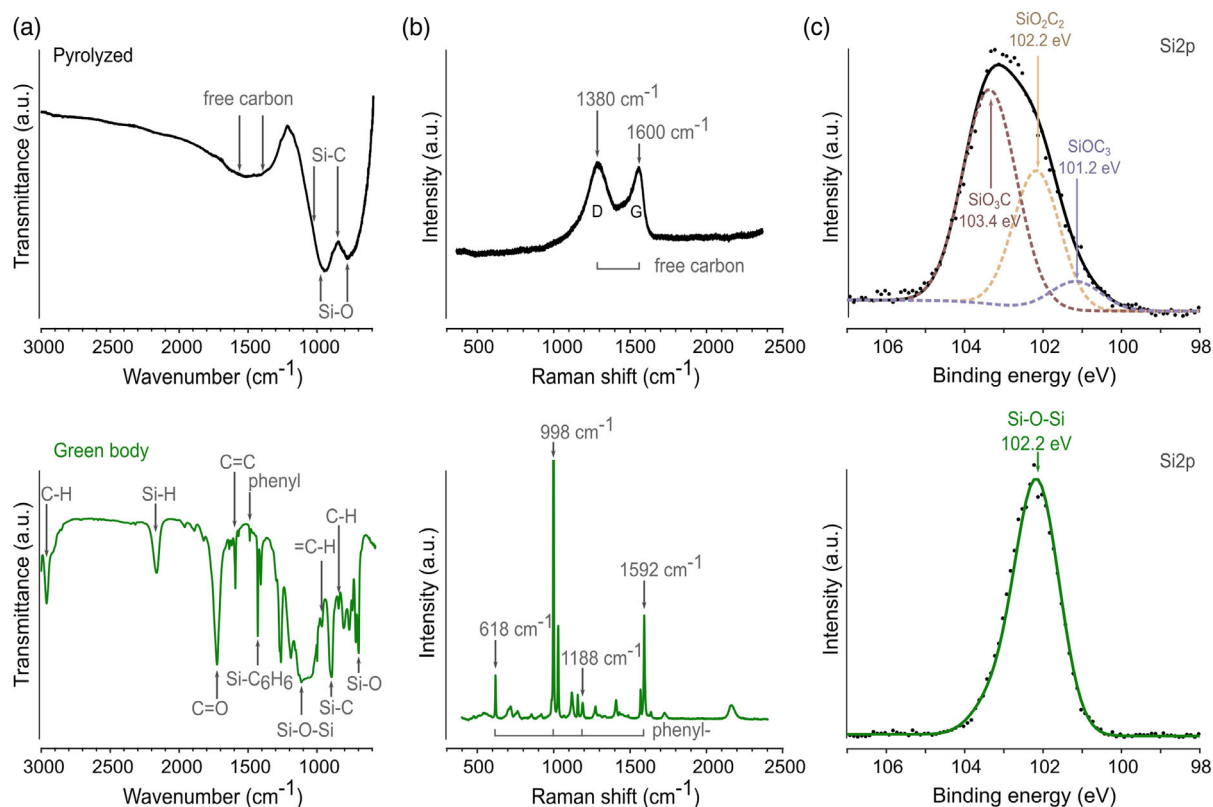


Figure 4. Pyrolysis leads to material transformation from organic green bodies (bottom) to ceramic pyrolyzed parts (top). a) FTIR spectra suggest conversion from the organic green body with numerous thin absorbance bands, many attributable to the organic bonds in the cross-linked PCP, to an inorganic silicon oxycarbide material, with Si—C and Si—O bonds. The absorbance region around 1500 cm^{-1} is attributable to the free carbon phase. b) Raman spectra corroborate the findings from FTIR. In the green body spectrum, four strong emission peaks match the spectral fingertip of the phenyl group present in the siloxane. In contrast, the pyrolyzed parts show a smoother emission spectrum, with two marked peaks representing the D and G bands of the free carbon phase. c) X-ray photoelectron spectra around the Si $2p$ bond. The spectrum for the pyrolyzed part spans the binding energies that are characteristic to intermediate mixed silicon oxycarbide species, namely, SiO_3C , SiO_2C_2 , and SiOC_3 . For the green body, the energy spectrum may be attributed to organic siloxanes.

Si—O—C network have been linked to higher pyrolysis temperatures. This free carbon, as illustrated in Figure 1b, has been suggested to explain the high thermal resistance of these materials.^[7] XPS spectra around the Si $2p$ bond show a broadening of the peak for the pyrolyzed parts, with respect to the green bodies, as shown in Figure 4c. The spectrum for the pyrolyzed part spans the binding energies that are characteristic to intermediate mixed silicon oxycarbide species, namely, SiO_3C , SiO_2C_2 , and SiOC_3 with binding energies at 103, 102, and 101 eV, respectively.^[49] Spectra at the O $1s$ and C $1s$ bonds are shown in Figure S6, Supporting Information. Bonds of lower energies, such as SiC,^[50] might be present in these samples, although at much lower concentrations, as the appearance of nanocrystalline SiC has been documented in PDCs only at higher pyrolysis temperatures ($>1300^\circ\text{C}$).^[31] Recent studies have shown that the site of binding between phenyl groups and the silicone backbone may result in mixed Si—O and Si—C bonding, particularly at the interface between the silica-rich nanodomains and the free carbon nanodomains.^[51] In contrast to the pyrolyzed state, the XPS spectrum of the Si $2p$ bond for the green

state shows a narrower peak, with an energy distribution that matches that of siloxanes with organic functional groups.^[52]

2.5. Resistance of 3D Printed Ceramic Parts

We tested the physical and chemical properties of the fabricated PDCs. To test their thermal resistance, we exposed the parts to rapid thermal shock cycles of 15 s heating up under the flame of a butane torch and 10 s of cooling down. The temperature of the flame ($T \approx 1400^\circ\text{C}$) is higher than the pyrolysis temperature. Figure 5a shows a time-lapse sequence of a spherical woodpile under its fifth thermal stress cycle. The first and last frames of the time-lapse show that the part retained its shape and did not crack, even withstanding the stress induced by the holding clamp. To assess the chemical inertness of the parts, we submerged them for 1 h in aqueous corrosive baths. Figure 5b shows a 3D cross PDC sitting in a HCl solution of pH = 2 on the left and a 3D cross PDC sitting in a KOH solution of pH = 14 on the right (see Figure S8, Supporting Information). Both parts

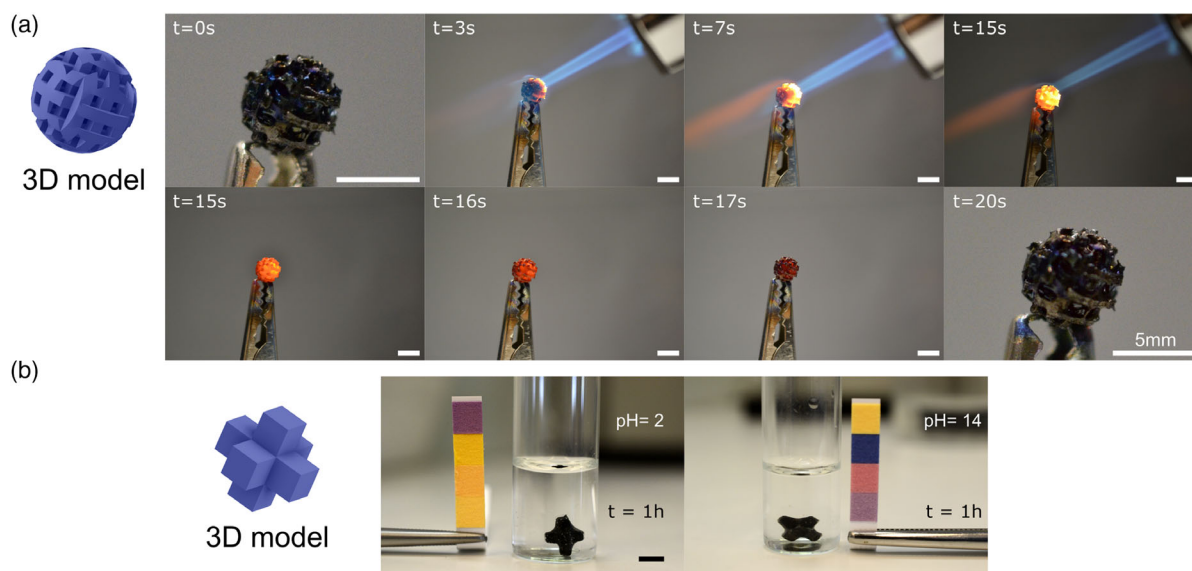


Figure 5. Resistance of 3D printed ceramic parts. a) Time-lapse of a ceramic part being heated to incandescence with a butane torch ($T \approx 1400^\circ\text{C}$) and then let cool down. The last frame shows the part after five cycles of thermal stress. Scale bar: 5 mm. b) Parts after being immersed for one hour in a strong acid ($\text{pH} = 2$) or a strong base ($\text{pH} = 14$) for 1 h. Scale bar: 2 mm.

retained their mass (within 0.1 mg on a precision scale). This demonstrates that they are very resistant to high temperatures, rapid heating and cooling for several cycles, and to corrosion.

3. Discussion and Conclusion

In this work, we demonstrated the fabrication of isotropic, fully dense, and crack-free PDCs from volumetric additive manufacturing. We formulated a transparent preceramic resin from a polysiloxane backbone and a diacrylate as a cross-linker. The resin was poured in a rotating cylindrical glass vial to be photocured with a laser source at 405 nm by using tomographic back projection. Parts with complex shapes were successfully fabricated and the green bodies were converted to ceramic parts through pyrolysis at 1000°C . We reported qualitatively on the density and the smoothness of the parts at the microscopic scale by micro-CT ($10\ \mu\text{m}$ resolution) and SEM (5 nm resolution). Based on experimental measurements, we report a mass loss of $54.0 \pm 0.2\%$ and a shrinkage of $31.0 \pm 1.7\%$ from green to pyrolyzed state. No significant anisotropy in shrinkage could be measured. We validated the polymer to ceramic conversion by FTIR, Raman, and XPS spectroscopy. We confirmed that the fabricated components exhibited strong resistance to thermal stress and to harsh chemical environments.

Ceramics are popular candidates for the fabrication of prototypes with exceptional properties, but traditional AM techniques impose long building time because of their inherent layer-by-layer process. Consequently, both steps of the 3D printing and the pyrolysis are time-consuming, which stands in the way of rapidly optimizing a ceramic prototype until specific requirements are met (accuracy, precision, and tolerance). Volumetric additive manufacturing is an emerging 3D printing technology that drastically accelerates the 3D printing step, leads to isotropic

shrinkage, and opens up a different range of materials and geometries for use in prototyping ceramics. Future work on assessing fabrication accuracy after pyrolysis could provide even faster cycles to optimize prototypes.

4. Experimental Section

The preceramic resin was prepared by combining a commercial polysiloxane $[\text{Si}(\text{C}_5\text{H}_6)_2\text{O}]_3[\text{Si}(\text{CH}_3)(\text{H})\text{O}]_2[\text{Si}(\text{CH}_3)(\text{CH}=\text{CH}_2)\text{O}]_2$, SPR 684, Starfire Systems, USA) with 1,4-butanediol diacrylate (BDDA) as a cross-linker (1070-70-8, Sigma-Aldrich, USA), and diphenyl (2,4,6-trimethylbenzoyl) phosphine oxide (TPO) as a photoinitiator (75 980-60-8, Sigma-Aldrich). The resin preparation consisted of 85 wt% polysiloxane, 15 wt% BDDA, and 2 mM TPO (0.063 wt%).

To produce the resin, TPO was diluted in BDDA to a concentration of $30\ \text{mg mL}^{-1}$ and vortexed. Following this, the polysiloxane precursor was combined with the TPO in the BDDA solution. The components were then simultaneously mixed and degassed using a planetary mixer (Mazerustar KK-250SE, Kurabo, Japan). Finally, the resin was poured into glass vials (diameter 16.5 mm), which were used for printing.

The absorbance spectra of the resin were measured with a Cary 50 (Varian, Australia) UV-vis spectrometer using a scan rate of $60\ \text{nm min}^{-1}$. The resin was poured in 10 mm plastic cuvettes. Before each analysis, a background acquisition was performed and then subtracted from the resin's spectra.

To evaluate the dose response of the resin, sets of millimetric cylinders were printed onto a static microscope slide. Each cylinder was printed with a different light dose. The coverslip was then imaged under an optical microscope (VHX-5000, Keyence VHX-5000, Japan). The cross-sectional area of each printed cylinder was digitally measured using the microscope. For each light dose, the polymerization ratio was calculated from the ratio between the printed cylinder's and the target's size.

The viscosity of the resin was measured using a rheometer (MCR 102, Anton-Paar, Austria) with a (25 mm) parallel plate and a gap of ($350\ \mu\text{m}$) at a shear rate of $0.108\ \text{Pa}$.

3D Printer. A custom volumetric 3D printer^[19] was used for this work. In it, the light from four laser diodes ($\lambda = 405\ \text{nm}$) was coupled into a

multimode fiber. Then, the beam was expanded to fill a Digital Micromirror Device, DMD, (VIS-7000, Vialux, Germany). The patterns for the tomographic reconstruction of the part were displayed on the DMD and projected by a pair of achromatic lenses with focal lengths of $f_1 = 100$ mm (AC254-100-A-ML, Thorlabs, USA) and $f_2 = 250$ mm (ACT508-250-A-ML, Thorlabs) onto the rotating cylindrical glass vial containing the photopolymer. The resin vial was dipped in a refractive index matching bath with square footprint to remove the lensing effects of the round vial. A camera records the progress of the print in the vial by imaging the sample with an orthogonal expanded laser beam ($\lambda = 671$ nm).

Tomographic Back Projection: The patterns for the tomographic back projection were computed following the algorithm described in the study by Loterie et al.^[19] To do so, the STL file of the 3D part was voxelized using a python script, which used binvox 3D mesh voxelizer as a backbone.^[53,54] Then, the Radon transform of this digital object was calculated over π radians around one of its axes. The Fourier transform of these patterns was taken and a ramp filter was applied to compensate for the over sampling of the low spatial frequencies. Finally, the inverse Fourier transform of these patterns was calculated. Additional corrections for attenuation from the photoinitiator were also performed following the study of Madrid-Wolff et al.^[22]

Printer Specifications: The photosensitive preceramic resin solidifies under a certain exposure to light, typically when the light dose reaches the polymerization threshold. To correctly print the object with a tomographic approach, it is important to project light from multiple angles which in practice corresponds to at least a few rotation of the vial. The rotation speed of the vial is set such that there is no flow of the resin during the print. In this work, the vial rotates 360° approximately 10 s and the number of rotations usually does not exceed 5–6. These are parameters that depend on the intensity of the light patterns and thus can be fine-tuned to improve the print quality. In our printer, the maximal printing resolution is around $80\ \mu\text{m}$. The minimal features of the final ceramic part are larger than the ones of the corresponding green body. This is due to pyrolysis that tends to deform and smooth the part. We estimate that the smallest feature one can obtain at the end of the complete fabrication process is around $200\ \mu\text{m}$.

After printing, the parts were recovered from the glass vials and dipped into a toluene bath, which was manually agitated for 5 min until all uncured resin dissolved. The parts were then placed in a bath of isopropyl alcohol (IPA) to dilute the toluene and stop the solving action on the parts. The bath was manually agitated again for 1 min. The parts were then left to dry in air at room temperature until all IPA fully evaporated, leaving them free of any unpolymerized resin.

The parts were then postcured in a UV curing station (FormCure, Formlabs, USA) for 1 h at room temperature. After this, all the remaining photoinitiator had been consumed, but the surface of the parts was still sticky. To remove the stickiness, green bodies were submerged in a concentrated solution of TPO in IPA ($10\ \text{mg mL}^{-1}$) and left for 1 h to allow TPO to diffuse inside. The bath with the parts was then placed for 15 min in the UV curing station. Then, the parts were removed from the bath and postcured dry one last time for 45 min in the curing station. After that, the green bodies were placed in an oven for 24 h at 80°C to remove any solvent that soaked into the part. Dry, postcured parts were kept in dry boxes until they were pyrolyzed.

The rinsed, postcured, and aged green bodies were then pyrolyzed in an alumina tube furnace (STF 15/450, Carbolite Gero, Germany) in a flowing argon atmosphere following the temperature profile described and explained in the Supporting Information. The pyrolysis peak temperature was set to $T = 1000^\circ\text{C}$, for a dwell time of 1 h, and a total cycle duration of 48 h. The detailed pyrolysis temperature profile is shown in Figure S3, Supporting Information.

μCT Imaging: Printed objects were imaged with voxel sizes of $10 \times 10 \times 10\ \mu\text{m}$ under a 160 kV X-ray transmission tomography (Hamamatsu, Japan). 3D visualizations and cross sections of the pieces were obtained using Fiji-ImageJ.^[55]

Photographic Imaging: Green bodies and pyrolyzed parts were imaged with a DSLR camera (D3100, Nikon, Japan) with a $f = 2.8$ macro lens (AF-S Micro Nikkor 40 mm, Nikon), and a digital microscope (VHX-5000, Keyence, USA) with magnifications between 20 and $100\times$.

SEM Imaging and Gold Deposition: The sputtering machine Alliance-Concept DP650 was used for the deposition of a thin gold layer (20 nm) on the samples. Following that, the samples were transferred to the SEM (SEM LEO 1550) and were inserted into the chamber vacuum for imaging the surface from low to high magnification. The resolution of this instrument was 5 nm.

To show resistance of the ceramic parts to high temperature, a butane torch was used to heat the ceramic parts ($T \approx 1400^\circ\text{C}$) for some seconds until they became incandescent and then let cool down. A typical thermal stress cycle was 20 s. The spherical woodpile shown in Figure 5 was subjected to five thermal stress cycles.

Parts were dipped into vials containing aqueous solutions of HCl and KOH solutions ($\text{pH} = 2$, and $\text{pH} = 14$, respectively) for 1 h and photographed at the beginning and the end of the experiment. The pH of the aqueous solutions was measured using 0–14 paper pH indicators (MQuant, Merck, Switzerland).

Raman spectra of the inside of green bodies and pyrolyzed parts were acquired with a LabRam HR800 spectrometer (HORIBA Scientific, USA) confocally coupled to an upright microscope (BX1, Olympus, Japan). To image the inside of the parts, green bodies were cut with a clean blade and pyrolyzed pieces were broken with a hammer. Samples were placed on microscope slides and excited at 532 nm (with a diode laser). Light was collected with a 10×0.25 NA air objective. Spectra were acquired using a grating with $1800\ \text{lines mm}^{-1}$, after three repetitions with integration times of 30 s. No postprocessing was performed on the data.

FTIR spectra of samples of parts in the green and pyrolyzed states were collected with a VERTEX 70v FT-IR Spectrometer (Bruker, USA). The spectrometer was coupled to a Hyperion upright microscope (Bruker). The sample of polymerized resin (green state) was prepared by depositing 50 of liquid preceramic resin on a gold mirror and spinning it at 6000 rpm. The sample was then polymerized under UV light for 5 min. The sample of pyrolyzed material was prepared by grinding pyrolyzed pieces with a mortar and a pestle until pulverized. The powder was resuspended in isopropyl alcohol. 100 of the suspension were deposited on a gold mirror and the alcohol was let to dry.

XPS measurements were performed using a Physical Electronics Versa Probe III system with a hemispherical analyzer and monochromated Al K α source. The energy scale linearity was calibrated with Au $4f_{7/2}$ at 84.00 eV and Cu $2p_{3/2}$ 932.62 eV. All data were measured at room temperature with a pass energy of 26 eV, at a takeoff angle of 45° and angular acceptance angle of $\pm 20^\circ$. The samples were electrically isolated during measurement and a low-energy Ar $^{+}$ and electron flood gun dual beam charge compensation system was used. The X-ray beam size on the sample was 100. Energy scale referenced to major C 1s peak at 284.8 eV which was assumed to originate primarily from C–C. No beam damage was observed.

To compare the differences between shrinkage along the axial and radial dimensions of the prints, a set of lengths were measured on green bodies and their corresponding PDCs ($n_{\text{parts}} = 7$, $n_{\text{measurements}} = 14$), most of them woodpiles. Flat geometries were chosen because they reduced ambiguity in measuring lengths, as shown in Figure S5, Supporting Information. Measurements were made from microscopic images acquired with an optical microscope (VHX-5000, Keyence).

Statistical analysis of the isotropy of shrinkage was conducted by running a two-tailed t -test assuming unequal variances (Welch test, $\alpha = 0.05$) on Microsoft Excel.

Supporting Information

Supporting Information is available from the Wiley Online Library or from the author.

Acknowledgements

M.K., G.K., and J.M.W. contributed equally to this work. The authors thank Lukas Riemer (Group for Ferroelectrics and Functional Oxides—EPFL) for his help with the pyrolysis and useful discussions. The authors also acknowledge Gary Perrenoud and the PIXE Facility at EPFL for the micro-CT scans of the parts. The authors acknowledge Dr. Siobhan McKeown of the Laboratory of Advanced Technology, Geneva, for her help with X-ray photoelectron spectroscopy and for the useful discussions and guidance analyzing the data, and Dr. Mounir Driss Mensi (X-Ray Diffraction and Surface Analytics Platform—EPFL), Dr. Pierre Mettraux (Molecular and Hybrid Materials Characterization Center—EPFL; in memoriam), and Dr. Nikolaos Nianias for their help with X-ray photoelectron spectroscopy. The authors thank Dr. Aleksanders Leitis and Deepthy Kavungal from the Bionanophotonic Systems Laboratory at EPFL for their help with Fourier-transform infrared spectroscopy (FTIR) and useful discussions. The authors thank Margarita Ariza-Acero at the University of Lausanne for help with Raman spectroscopy. The authors thank the large number of open projects that facilitated this work, including FreeCAD, ImageJ, Python, Anaconda, Binvox, and Inkscape. This work was supported by the Strategic Focus Area from the ETH Domain (SFA)- Advanced Manufacturing for the Ceramic X.0 -High-precision micro-manufacturing of ceramics, and by the Swiss National Science Foundation under project number 196971 - “Light based Volumetric printing in scattering resins”

Open access funding provided by Ecole Polytechnique Federale de Lausanne.

[Correction added on April 7, 2022, after first online publication: CSAL funding statement has been added.]

Conflict of Interest

Dr. D. Loterie and Dr. P. Delrot are shareholders and employees of Readily3D SA. Prof. C. Moser is a shareholder of Readily3D SA. All the other co-authors declare no conflicts of interest.

Data Availability Statement

Data are also freely available from the Zenodo repository under DOI 10.1002/adem.202101345.

Keywords

ceramics, 3D printing, polymer-derived ceramics, preceramic polymers, SiOC, volumetric additive manufacturing

Received: September 30, 2021

Revised: December 11, 2021

Published online:

- [1] P. Greil, *Adv. Eng. Mater.* **2002**, 4, 247.
- [2] R. Janssen, S. Scheppokat, N. Claussen, *J. Eur. Ceram. Soc.* **2008**, 28, 1369.
- [3] R. He, W. Liu, Z. Wu, D. An, M. Huang, H. Wu, Q. Jiang, X. Ji, S. Wu, Z. Xie, *Ceram. Int.* **2018**, 44, 3412.
- [4] S. Fu, M. Zhu, Y. Zhu, *J. Adv. Ceram.* **2019**, 8, 457.
- [5] D. De Faoite, D. J. Browne, F. R. Chang-Díaz, K. T. Stanton, *J. Mater. Sci.* **2012**, 47, 4211.
- [6] E. Zanchetta, M. Cattaldo, G. Franchin, M. Schwentenwein, J. Homa, G. Brusatin, P. Colombo, *Adv. Mater.* **2016**, 28, 370.
- [7] P. Colombo, G. Mera, R. Riedel, G. D. Sorarù, *J. Am. Ceram. Soc.* **2010**, 93, 1805.
- [8] L.-A. Liew, Y. Liu, R. Luo, T. Cross, L. An, V. M. Bright, M. L. Dunn, J. W. Daily, R. Raj, *Sens. Actuators A: Phys.* **2002**, 95, 120.
- [9] D. A. Walker, J. L. Hedrick, C. A. Mirkin, *Science* **2019**, 366, 360.
- [10] G. Mera, A. Navrotsky, S. Sen, H.-J. Kleebe, R. Riedel, *J. Mater. Chem. A* **2013**, 1, 3826.
- [11] M. Schwentenwein, P. Schneider, J. Homa, in *Advances in Science and Technology*, vol. 88, Trans Tech Publications Ltd, Switzerland **2014**, pp. 60–64.
- [12] J. Schmidt, P. Colombo, *J. Eur. Ceram.* **2018**, 38, 57.
- [13] T. A. Pham, D.-P. Kim, T.-W. Lim, S.-H. Park, D.-Y. Yang, K.-S. Lee, *Adv. Funct. Mater.* **2006**, 16, 1235.
- [14] L. Brigo, J. E. M. Schmidt, A. Gandin, N. Michieli, P. Colombo, G. Brusatin, *Adv. Sci.* **2018**, 5, 1800937.
- [15] G. Konstantinou, E. Kakkava, L. Hagelüken, P. V. Warriam Sasikumar, J. Wang, M. G. Makowska, G. Blugan, N. Nianias, F. Marone, H. Van Swygenhoven, J. Brugger, D. Psaltis, C. Moser, *Addit. Manuf.* **2020**, 35, 101343.
- [16] M. Mahmoudi, C. Wang, S. Moreno, S. R. Burlison, D. Alatalo, F. Hassanipour, S. E. Smith, M. Naraghi, M. Minary-Jolandan, *ACS Appl. Mater. Interfaces* **2020**, 12, 31984.
- [17] B. E. Kelly, I. Bhattacharya, H. Heidari, M. Shusteff, C. M. Spadaccini, H. K. Taylor, *Science* **2019**, 363, 1075.
- [18] P. N. Bernal, P. Delrot, D. Loterie, Y. Li, J. Malda, C. Moser, R. Levato, *Adv. Mater.* **2019**, 31, 1904209.
- [19] D. Loterie, P. Delrot, C. Moser, *Nat. Commun.* **2020**, 11, 1.
- [20] M. Regehy, Y. Garmshausen, M. Reuter, N. F. König, E. Israel, D. P. Kelly, C.-Y. Chou, K. Koch, B. Asfari, S. Hecht, *Nature* **2020**, 588, 620.
- [21] C. C. Cook, E. J. Fong, J. J. Schwartz, D. H. Porcincula, A. C. Kaczmarek, J. S. Oakdale, B. D. Moran, K. M. Champley, C. M. Rackson, A. Muralidharan, R. R. McLeod, M. Shusteff, *Adv. Mater.* **2020**, 32, 2003376.
- [22] J. Madrid-Wolff, A. Boniface, D. Loterie, P. Delrot, C. Moser, Light-based volumetric additive manufacturing in scattering resins, arXiv preprint arXiv:2105.14952, **2021**.
- [23] J. Lalevée, J.-P. Fouassier, *Dyes and Chromophores in Polymer Science*, John Wiley & Sons, Hoboken **2015**.
- [24] A. Eibel, D. E. Fast, G. Gescheidt, *Polym. Chem.* **2018**, 9, 5107.
- [25] S. C. Ligon, B. Husár, H. Wutzel, R. Holman, R. Liska, *Chem. Rev.* **2014**, 114, 557.
- [26] P. J. Flory, *J. Am. Chem. Soc.* **1941**, 63, 3083.
- [27] J. Kaspar, M. Graczyk-Zajac, R. Riedel, *Solid State Ionics* **2012**, 225, 527.
- [28] S. Martínez-Crespiera, E. Ionescu, H.-J. Kleebe, R. Riedel, *J. Eur. Ceram. Soc.* **2011**, 31, 913.
- [29] M. Makowska, P. V. W. Sasikumar, L. Hagelüken, D. F. Sanchez, N. Casati, F. Marone, G. Blugan, J. Brugger, H. Van Swygenhoven, *Acta Mater.* **2020**, 198, 134.
- [30] G. Liu, J. Kaspar, L. M. Reinold, M. Graczyk-Zajac, R. Riedel, *Electrochim. Acta* **2013**, 106, 101.
- [31] J. Kaspar, M. Graczyk-Zajac, R. Riedel, *J. Power Sources* **2013**, 244, 450.
- [32] S. Shoji, S. Kawata, *Appl. Phys. Lett.* **1999**, 75, 737.
- [33] C. Rackson, R. McLeod, *Volumetric Additive Manufacturing Workshop*, August 2021, Virtual workshop, <https://web.cvent.com/event/bfa9acd7-695a-4f1d-a249-832b0c858f55/>.
- [34] J. M. Hundley, Z. C. Eckel, E. Schueller, K. Cante, S. M. Biesboer, B. D. Yahata, T. A. Schaedler, *Addit. Manuf.* **2017**, 18, 95.
- [35] U. K. Roopavath, S. Malferrari, A. Van Haver, F. Verstreken, S. N. Rath, D. M. Kalaskar, *Mater. Des.* **2019**, 162, 263.
- [36] M. Graczyk-Zajac, L. Toma, C. Fasel, R. Riedel, *Solid State Ionics* **2012**, 225, 522.
- [37] P. V. W. Sasikumar, G. Blugan, N. Casati, E. Kakkava, G. Panusa, D. Psaltis, J. Kuebler, *Ceram. Int.* **2018**, 44, 20961.

- [38] A. Sonseca, M. El Fray, *RSC Adv.* **2017**, 7, 21258.
- [39] B. Smith, *Spectroscopy* **2016**, 31, 34.
- [40] P. Beauchamp, Spectroscopy tables, n.d., https://www.cpp.edu/~psbeauchamp/pdf/spec_ir_nmr_spectra_tables.pdf (accessed: January 2022).
- [41] W. Guodong, S. Yongcai, L. Yongqiang, *RSC Adv.* **2018**, 8, 21863.
- [42] P. J. Launer, B. Arkles, in *Silicon Compounds*, 3rd ed., Gelest Inc., Morrisville, PA **2013**, pp. 175–178.
- [43] A. Łapiński, J. Spanget-Larsen, M. Langgård, J. Waluk, J. G. Radziszewski, *J. Phys. Chem. A* **2001**, 105, 10520.
- [44] L. B. Capeletti, I. M. Baibich, I. S. Butler, J. H. Z. Dos Santos, *Spectrochim. Acta, Part A* **2014**, 133, 619.
- [45] D. S. Knight, W. B. White, *J. Mater. Res.* **1989**, 4, 385.
- [46] T. Jiang, Y. Wang, Y. Wang, N. Orlovskaya, L. An, Y. Wang, Y. Wang, N. Orlovskaya, L. An, *J. Am. Ceram. Soc.* **2009**, 92, 2455.
- [47] P. Dibandjo, M. Graczyk-Zajac, R. Riedel, V. S. Pradeep, G. D. Soraru, *J. Eur. Ceram. Soc.* **2012**, 32, 2495.
- [48] A. B. Kousaalya, X. Zeng, M. Karakaya, T. Tritt, S. Pilla, A. M. Rao, *ACS Appl. Mater. Interfaces* **2018**, 10, 2236.
- [49] G. D. Sorarù, G. D'andrea, A. Glisenti, *Mater. Lett.* **1996**, 27, 1.
- [50] R. Corriu, D. Leclercq, P. Mutin, A. Vioux, *J. Sol-Gel Sci. Technol.* **1997**, 8, 327.
- [51] C. Sugie, A. Navrotsky, S. Lauterbach, H.-J. Kleebe, G. Mera, *Materials* **2021**, 14, 4075.
- [52] J. A. Gardella Jr., S. A. Ferguson, R. L. Chin, *Appl. Spectrosc.* **1986**, 40, 224.
- [53] F. S. Nooruddin, G. Turk, *IEEE Trans. Visual Comput. Graphics* **2003**, 9, 191.
- [54] P. Min, Binox 3D mesh voxelizer, **2004–2019**, <http://www.patrickmin.com/binvox>; <https://www.google.com/search?q=binvox>, (accessed: January 2021).
- [55] J. Schindelin, I. Arganda-Carreras, E. Frise, V. Kaynig, M. Longair, T. Pietzsch, S. Preibisch, C. Rueden, S. Saalfeld, B. Schmid, J.-Y. Tinevez, D. J. White, V. Hartenstein, K. Eliceiri, P. Tomancak, A. Cardona, *Nat. Methods* **2012**, 9, 676.